DE82014980

HEAT AND MASS TRANSFER EFFECT IN SLURRY BED FISCHER-TROPSCH REACTORS

CALIFORNIA UNIV., BERKELEY. LAWRENCE BERKELEY LAB

FEB 1982

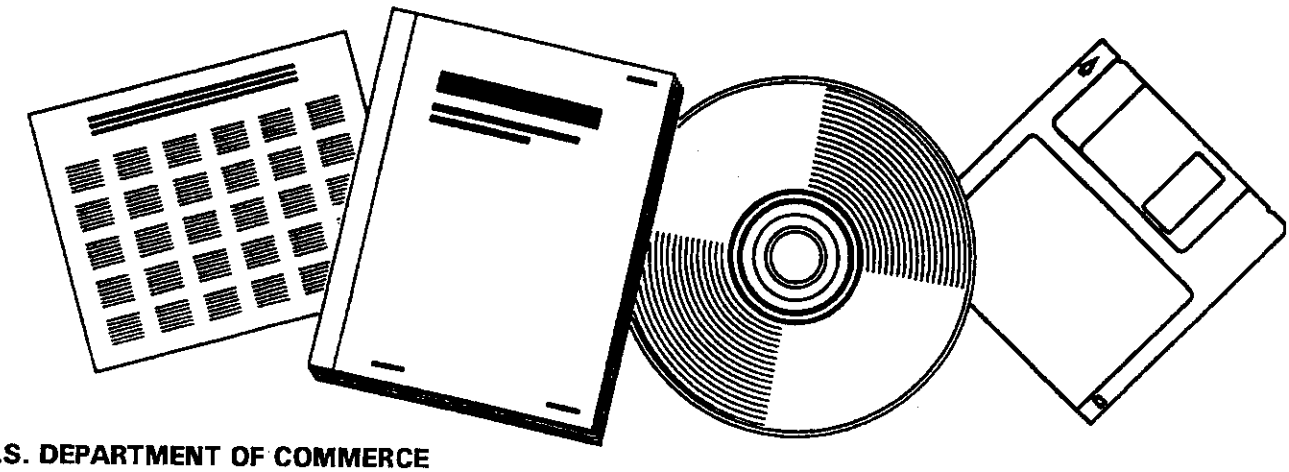

U.S. DEPARTMENT OF COMMERCE
National Technical Information Service

LBL--13238 Rev.

DE82 014980

HEAT- AND MASS-TRANSFER EFFECT IN SLURRY-BED FISCHER-TROPSCH REACTORS

HEINEMANN, H.,[1] BELL, A. T.,[2] and STERN, D.A.
Ph. D.[1] (Basel), D. Sc. (MIT)[2]
[1]Lawrence Berkeley Laboratory, University of California
[2]Chemical Engineering Department, University of California

Applied Catalysis, in press
Chemical Engineering Science, in press

SYNOPSIS

Fischer-Tropsch Reactions can be carried out in fixed bed, fluid bed, and slurry bed reactors. One of the advantages claimed for slurry bed reactors is the ability to operate at lower hydrogen to carbon monoxide ratios than the other two reactors. Reasons for this difference have not previously been fully established. The present investigation has concentrated on two factors which may contribute to the ability of the slurry reactor to tolerate lower hydrogen/CO ratios. These are: (1) greater isothermicity, and (2) mass transfer effects on the gas-liquid interface in the slurry reactor. Work with small diameter fixed bed reactors has shown that there is a critical temperature at which plugging of the reactors using an iron catalyst will occur. The exact temperature is a function of both the hydrogen/CO ratio and the space velocity. A difference of 10 to 15°C separates operability from non-operability. It is therefore likely that in the critical temperature range around 300°C hot spots on the catalyst may be the cause of plugging and deactivation at low hydrogen/CO ratios and that such hot spot development can be inhibited by operation in the liquid phase.

This work was supported by the Assistant Secretary of Fossil Energy, Office of Coal Research, University Contracts Division of the U.S. Department of Energy under Contract Number DE-AC03-76SF00098.

MGW

The influence of mass transfer on the hydrogen/CO ratio in the liquid phase of a slurry reactor has been analyzed theoretically, again using an iron catalyst. The basis for the model was the operation of an experimental slurry reactor. It was determined that even under circumstances where the gas-liquid mass transfer resistance is a small fraction of the over-all resistance, differences in the solubilities and diffusivities of hydrogen and carbon monoxide can give rise to liquid phase hydrogen/CO ratios which differ substantially from that of the gas fed to the reactor. The direction and magnitude of the change in the liquid phase ratio is dependent on the consumption ratio of hydrogen respectively carbon monoxide, the interfacial area for mass transfer from the bubble face, the Damkohler number and the space velocity of the feed gas.

Because of space limitations only the reactor model is described in this preprint.

NOMENCLATURE

a	Bubble interfacial area per unit reactor volume (cm^{-1})
$C_{G,i}$	Gas-phase concentration of component i (mol/cm^3)
$G_{L,i}$	Liquid-phase concentration of component i (mol/cm^3)
Da	Damkohler number
$D_{L,i}$	Liquid-phase diffusivity of component i (cm^2/s)
k_o	Rate coefficient (s^{-1})
$k_{L,i}$	Liquid-phase mass-transfer coefficient for component i (cm^2/s)
L	Reactor length (cm)
m_i	Solubility coefficient for component i
N_i	Stanton number for component i
Q_L	Liquid-phase flow rate (cm^3/s)
r_i	Rate of formation of consumption of component i (mol/cm^3s)
U_G	Superficial gas velocity (cm/s)
V_r	Reactor volume (cm^3)
w	Catalyst loading (g/cm^3)
z	Distance from the gas inlet (cm)
ϵ_G	Fraction of total reactor volume occupied by bubbles
ζ	Dimensionless axial distance
η	Column efficiency
Θ_G	Dimensionless gas-phase concentration
$\Theta_{G,i}$	Dimensionless gas-phase concentration of component i
$\Theta_{L,i}$	Dimensionless liquid-phase concentration of component i
μ_L	Liquid viscosity (cp)
ν_i	Stoichiometric coefficient for component i
ρ_L	Liquid density (g/cm^3)
τ_G	Gas space time (s)
τ_L	Liquid space time (s)
υ	Dimensionless gas velocity

REACTOR MODEL

The following assumptions were introduced to simplify the reactor model: (1) the liquid phase is well-mixed; (2) the catalyst is uniformly dispersed; (3) the gas is in plug flow; (4) the primary resistance to mass transfer is at the gas-liquid interface. It was further assumed that there is a small, but constant, flow of liquid into and out of the column.

The gas-phase mass balance for each component, written over a differential element of the reactor, is given by

$$-\frac{d(U_G C_{G,i})}{dz} = k_{L,i}a(C^*_{L,i} - C_{L,i}) \tag{1}$$

where $C^*_{L,i} = C_{G,i}/m_i$. To account for changes in gas velocity with position in the column, one must also consider an overall mass balance, given by

$$-C_G \frac{dU_G}{dz} = \sum_{i=1}^{n} k_{L,i}a(C^*_{L,i} - C_{L,i}) \tag{2}$$

The boundary conditions on Eqs. 1 and 2, defined at $z = 0$, are

$$U_G = U^o_G$$

$$C_{G,i} = C^o_{G,i} \tag{3}$$

The liquid-phase mass balance for each component, assuming that no reactant or product enters with the liquid, can be written as

$$-Q_L C_{L,i} + \int_o^{V_r} k_{L,i}a(C^*_{L,i} - C_{L,i})\, dV_r = V_r w(1 - \epsilon_G)\, r_i \tag{4}$$

If the average gas phase concentration for each component is defined as

$$\bar{C}_{G,i} = \frac{1}{V_r}\int_o^{V_r} C_{G,i} dV_r \quad , \tag{5}$$

then Eq. 4 can be written as

$$-Q_L C_{1,i} + V_r k_{L,i} a(\bar{C}^*_{L,i} - C_{L,i}) = V_r w(1 - \epsilon_G)\, r_i \qquad (6)$$

Equations 1, 2, 5 and 6 are non-dimensionalized by use of the following definitions

$$\theta_{G,i} = C_{G,i}/C^o_{G,H_2} \qquad \nu = U_G/U^o_G$$

$$\theta_{L,i} = C_{L,i} m_i / C^o_{G,H_2} \qquad \tau_G = L/U^o_G \qquad (7)$$

$$\theta_G = C_G/C^o_{G,H_2} \qquad \tau_L = V_r/Q_L$$

$$\zeta = z/L \qquad N_i = \frac{k_{L,i} a\, L}{m_i U^o_G}$$

Thus,

$$-\frac{d(\nu\theta_{G,i})}{d\zeta} = N_i(\theta_{G,i} - \theta_{L,i}) \qquad (8)$$

$$-\theta_G \frac{d\nu}{d\zeta} = \sum_{i=1}^{n} N_i(\theta_{G,i} - \theta_{L,i}) \qquad (9)$$

$$-\theta_{G,i} = \int_0^1 \theta_{G,i}\, d\zeta \qquad (10)$$

$$-\theta_{L,i} + N_i \frac{m_i \tau_L}{\tau_G}(\bar{\theta}_{G,i} - \theta_{L,i}) = \frac{m_i V_r w(1 - \epsilon_G)\, r_i}{Q_L C^o_{G,H_2}} \qquad (11)$$

The dimensionless group N_i appearing in Eqs. 8, 9, 11 is the Stanton number for component i and represents the ratio of the gas space time to the characteristic time for liquid-phase mass transfer.

Studies by several groups have shown that the kinetics of methane synthesis and CO consumption over iron catalysts are, to a good approximation, first order in H_2 concentration and zero order in CO concentration. Accordingly, the rate of formation or consumption of component i can be represented by

$$r_i = \nu_i K_0 C_{L,H_2} \tag{12}$$

Substitution of Eq. 12 into Eq. 11, allows us to rewrite Eq. 11 as

$$-\theta_{L,i} + N_i m_i \frac{\tau_L}{\tau_G}(\bar{\theta}_{G,i} - \theta_{L,i}) = \nu_i Da \frac{\tau_L}{\tau_G} \frac{m_i}{m_{H_2}} \theta_{L,H_2} \tag{13}$$

The dimensionless group Da appearing in Eq. 13 is the Damkohler number, which is defined as

$$Da = \frac{Lw(1-\epsilon_G)\, k_o}{U_G^o} \tag{14}$$

Numerical Methods

Equations 8-10 and 13, together with the boundary conditions given by Eq. 3, were solved numerically. The function f_i was defined by adding the right-hand-side of Eq. 13 to its left-hand-side. A zero solution to f_i was then sought by a regula-falsi technique. Convergence was accepted when the values of $C_{L,i}$ used to predict new $C_{L,i}$ were within 1 percent.

RESULTS AND DISCUSSION

Figure 1 illustrates the axial concentration profiles for each component in both the gas and liquid phases, for the case in which $\tau_G = 70$ s and $\tau_L = 700$ s and for the reaction $2H_2 + CO \rightleftharpoons CH_4 + CO_2$. The gas-phase concentration of H_2 falls off very rapidly near the entrance to the column and for $\zeta > 0.4$ approaches a nearly constant value, approximating that corresponding to equilibrium with the liquid-phase concentration of H_2. The decrease in the gas-phase concentration of CO with increasing ζ is much less rapid than that for H_2, and equilibrium between the gas-phase CO concentration is not attained at any point in the column. This difference in the gas-phase concentration profiles is attributable to the significantly larger mass-transfer coefficient for H_2 than for CO.

The gas phase concentration profiles for CH_4 and CO_2 are similar in shape but the concentration of CH_4 exceeds that of CO_2 over a major portion of the column. This relationship can be ascribed to the fact that the

mass-transfer coefficient for CH_4 is larger than that for CO_2. It is of further interest to note that for $\zeta \gtrsim 0.5$, the dimensionless gas-phase concentrations for CH_4 and CO_2 exceed the dimensionless liquid-phase concentrations for these components. The following explanation can be given for this pattern. As gas bubbles travel up the column, their content of CH_4 and CO_2 increases due to mass transfer from the liquid phase. The gas-phase concentration of these components also increases due to the depletion of H_2 and CO from the bubbles. It is this latter effect, coupled with the relatively slow mass transfer rates associated with CH_4 and CO_2, which permits the gas-phase concentrations of CH_4 and CO_2 to exceed the level expected for equilibrium with the liquid-phase concentrations of these components.

An important consequence of the difference in the mass-transfer rates of different components is that the H_2/CO ratio in the liquid phase is greater than that in the gas feed. This results directly from the fact that while the fluxes of CO and H_2 to the surface of the catalyst particles are identical, the liquid-phase gradient for H_2 is much smaller than that for CO.

The influence of a reduction in the gas-phase space time to 35 s is shown in Fig. 2. In performing the calculations shown in this figure, it was assumed that both ε_G and a are independent of gas velocity. This assumption is supported by the experimental observations reported by Calderbank et al. (2) for $U_G > 4$ cm-sec^{-1}. As a result of the lower space time, the gas-phase concentrations presented in Fig. 2 change more slowly with ζ than those shown in Fig. 1, but otherwise the trends observed in both figures are qualitatively the same. Comparison of the liquid-phase H_2/CO ratio for the two gas-phase space velocities shows that the ratio is higher for the lower space velocity. Thus, $C_{L,H_2}/C_{L,CO} = 2.75$ for $\tau_G = 35$ s, and $C_{L,H_2}/C_{L,CO} = 1.67$ for $\tau_G = 70$ s. This difference can be explained in terms of the differences in the gas-phase concentration profiles for the two cases. For $\tau_G = 35$ s, the gas-phase concentrations for H_2 and CO deviate to a lesser degree than for $\tau_G = 70$ s. As a consequence, the liquid-phase concentrations of H_2 and CO must differ by a more significant degree for the lower space time, in order to maintain the required relative driving forces for mass transfer through the liquid phase. For $\tau_G = 70$ s, the average CO

concentration in the gas phase is much higher than the average H_2 concentration, and, consequently, the liquid phase concentrations of H_2 and CO need not differ by as much to satisfy the liquid-phase mass balance.

The extent to which the H_2/CO ratio in the liquid phase exceeds that fed to the column in the gas phase is a strong function of the relative magnitudes of k_{L,H_2} and $k_{L,CO}$, as shown in Fig. 3. The two curves shown in this figure were generated by varying k_{L,H_2}, holding $k_{L,CO}$ and all other parameters constant. The H_2/CO ratio at $N_{L,H_2} = N_{L,CO}$ depends on the feed H_2/CO ratio as well as the ratio of H_2 to CO consumption during synthesis. For the case under consideration, both the feed ratio and the consumption ratio are unity and, hence, the liquid-phase H_2/CO ratio becomes 0.76, the ratio of the solubilities of H_2 and CO. As the value of $N_{L,H_2}/N_{CO}$ increases above unity, the H_2/CO ratio in the liquid phase rises rapidly and then passes through a broad maximum. This trend, which is different for each value of τ_G, can be explained in terms of the effect of increasing k_{L,H_2} on the axial-concentration profiles for H_2 and CO. As k_{L,H_2} increases, the H_2 profile falls progressively below that for CO, as a consequence of the increased rate of H_2 mass transfer. This causes the liquid-phase concentration of H_2 to rise above that for CO. Eventually, the liquid-phase H_2 concentration rises to the point where it is in equilibrium with the exiting gas phase concentration.

The influence of the ratio of the solubility constants for H_2 and CO on the H_2/CO ratio in the liquid phase is shown in Fig. 4. The solid curve traces the effects of m_{H_2}/m_{CO} on $C_{L,H_2}/C_{L,CO}$ in the presence of mass transfer effects, and the dashed line indicates what would occur in the absence of any mass-transfer limitations. It is apparent that as the solubility of H_2 relative to CO increases (i.e., m_{CO}/m_{H_2}), mass-transfer effects have an increasingly larger affect on the liquid-phase ratio of H_2 to CO.

The stoichiometric relationship between the rates of H_2 and CO consumption depends upon the nature of the products produced. In the example considered thus far, it has been assumed that CH_4 and CO_2 are the principal products and, hence, that equivalent quantities of H_2 and CO are

consumed. If, on the other hand, one considers that olefins and CO_2 are the primary products, then twice as much CO as H_2 will be consumed. Figure 5 shows the effects of varying $k_{L_1H_2}$, keeping all other parameters constant on $C_{L,H_2}/C_{L,CO}$ for the case in which pentene is taken as a typical olefin product. It is apparent that the H_2/CO ratio in the liquid phase can be substantially greater than the ratio in the feed gas, 0.67, and that the maximum enhancement in the liquid-phase H_2/CO ratio is greater in this case than in the case where CH_4 is the primary hydrocarbon product (see Fig. 1). Both of these observations are a direct result of the fact that the consumption of CO exceeds the consumption of H_2. It is interesting to note that the liquid H_2/CO ratio does not go through a maximum as k_{L,H_2} increases. Since the feed concentration of CO is high, changes in the gas phase CO concentration profile have only a small effect on the driving force for transfer of CO, and as a consequence the liquid-phase concentration of CO does not increase noticeably at high values of k_{L,H_2}.

CONCLUSIONS

The present analysis has shown that the H_2/CO ratio in the liquid phase of a slurry reactor used for Fischer-Tropsch synthesis is a sensitive function of differences in the solubilities and mass-transfer coefficients for H_2 and CO, and that the liquid-phase H_2/CO ratio can differ substantially from that of the gas fed to the reactor. In addition to the factors mentioned, the direction and magnitude of the change in liquid-phase H_2/CO ratio is dependent on the H_2/CO consumption ratio, the interfacial area, the Damkohler number, and the space velocity of the feed gas. It has been demonstrated that the influence of mass-transfer effects on the liquid-phase H_2/CO ratio can be large even under circumstances where the gas-liquid mass-transfer resistance is a relatively small fraction of the overall reaction resistance. Since the liquid-phase H_2/CO ratio influences the average molecular weight of the products formed, the olefin to paraffin ratio of the products, and the formation of free carbon, knowledge of the dependence of the H_2/CO ratio on reaction conditions should be taken into account in the design of slurry columns used for Fischer-Tropsch synthesis.

ACKNOWLEDGMENT

This work was supported by the Assistant Secretary of Fossil Energy, Office of Coal Research, University Contracts Division of the U.S. Department of Energy under Contract Number DE-AC03-76SF00098.

FIGURE CAPTIONS

Figure 1. Dependence of $\theta_{G,i}$ and $\theta_{L,i}$ on ζ for the reaction $2H_2 + 2CO \rightarrow CH_4 + CO_2$: $\tau_G = 70$ s; $\tau_L = 700$ s; $N_{H_2} = 13.20$; $N_{CO} = 1.57$; $N_{CH_4} = 7.41$; $N_{CO_2} = 4.41$.

Figure 2. Dependence of $\theta_{G,i}$ and $\theta_{L,i}$ on ζ for the reaction $2H_2 + 2CO \rightarrow CH_4 + CO_2$: $\tau_G = 35$ s; $\tau_L = 700$ s; $N_{H_2} = 6.60$; $N_{CO} = 0.79$; $N_{CH_4} = 3.71$; $N_{CO_2} = 2.21$.

Figure 3. Dependence of $C_{L,H_2}/C_{L,CO}$ on k_{L,H_2} and τ_G for the reaction $2H_2 + 2CO \rightarrow CH_4 + CO_2$.

Figure 4. Dependence of $C_{L,H_2}/C_{L,CO}$ on $m_{H_2}^{-1}$ for the reaction $2H_2 + 2CO \rightarrow CH_4 + CO_2$: $\tau_G = 70$ s; $\tau_L = 700$ s; $N_{CO} = 1.51$; $N_{CH_4} = 7.41$; $N_{CO_2} = 4.41$.

Figure 5. Dependence of $C_{L,H_2}/C_{L,CO}$ on k_{L,H_2} for the reaction $10\ CO + 5\ H_2 \rightarrow C_5H_{10} + 5\ CO_2$; $\tau_G = 70$ s; $\tau_L = 700$ s; $N_{CO} = 1.57$; $N_{C_5H_{10}} = 2.80$; $N_{CO_2} = 4.41$.

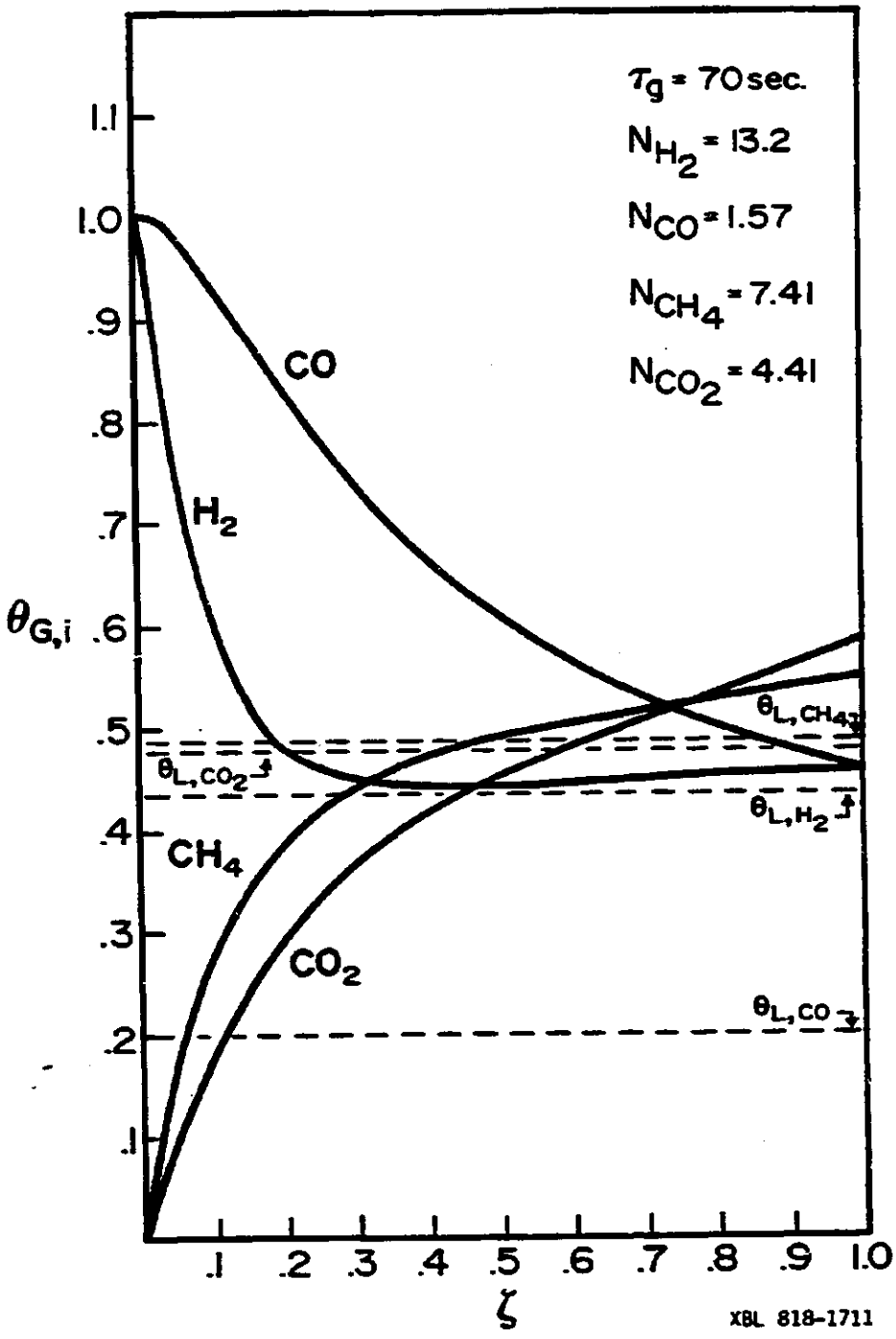
τ_g = 70 sec.
N_{H_2} = 13.2
N_{CO} = 1.57
N_{CH_4} = 7.41
N_{CO_2} = 4.41
CO
H_2
CH_4
CO_2
$\theta_{G,i}$
θ_{L,CH_4}
θ_{L,CO_2}
θ_{L,H_2}
$\theta_{L,CO}$
1.1
1.0
.9
.8
.7
.6
.5
.4
.3
.2
.1
.1 .2 .3 .4 .5 .6 .7 .8 .9 1.0
ζ
XBL 818-1711

Figure 1

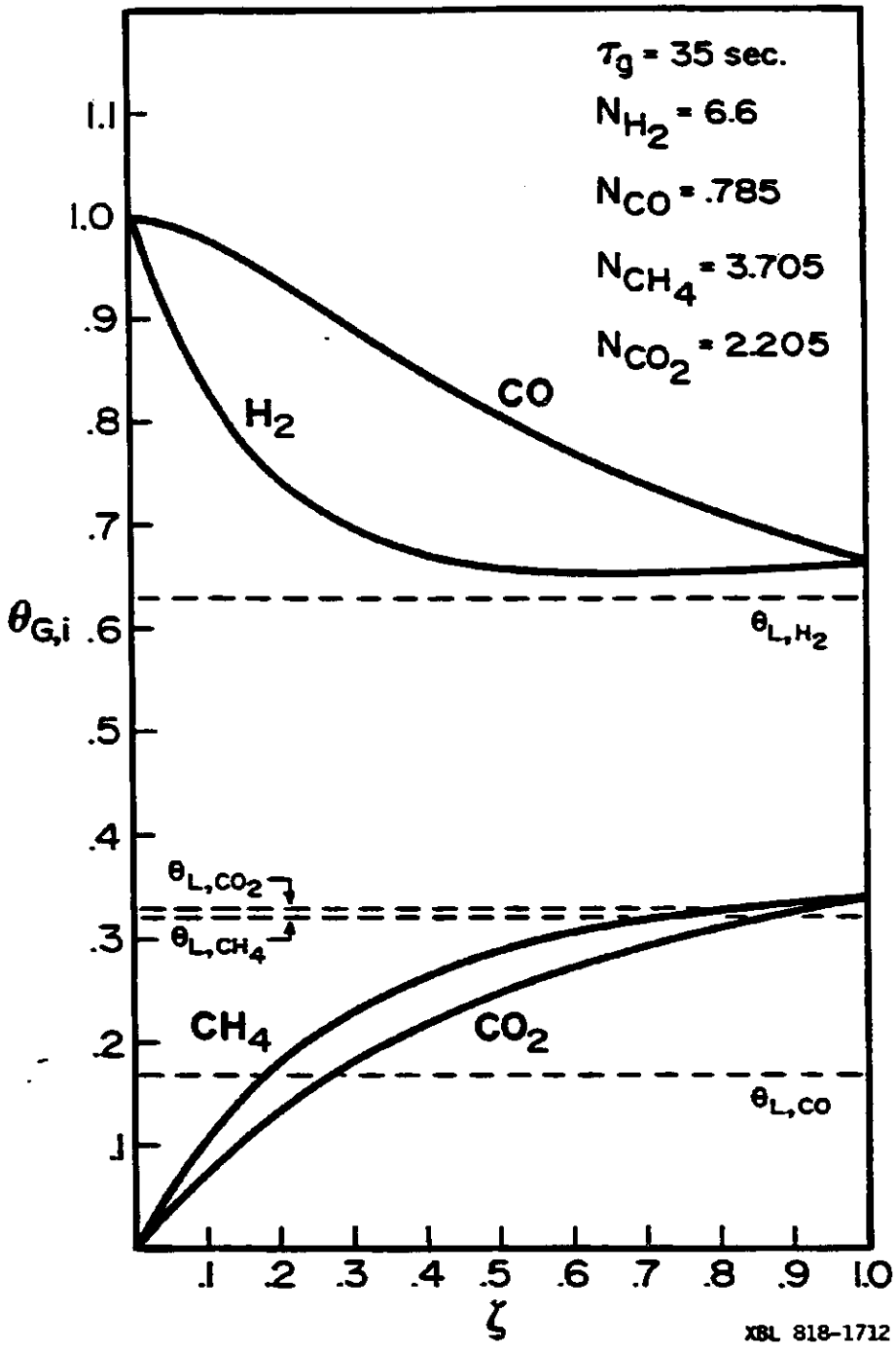
τ_g = 35 sec.
N_{H_2} = 6.6
N_{CO} = .785
N_{CH_4} = 3.705
N_{CO_2} = 2.205
CO
H_2
θ_{L,H_2}
θ_{L,CO_2}
θ_{L,CH_4}
CH_4
CO_2
$\theta_{L,CO}$
$\theta_{G,i}$
1.1
1.0
.9
.8
.7
.6
.5
.4
.3
.2
.1
.1 .2 .3 .4 .5 .6 .7 .8 .9 1.0
ζ
XBL 818-1712

Figure 2

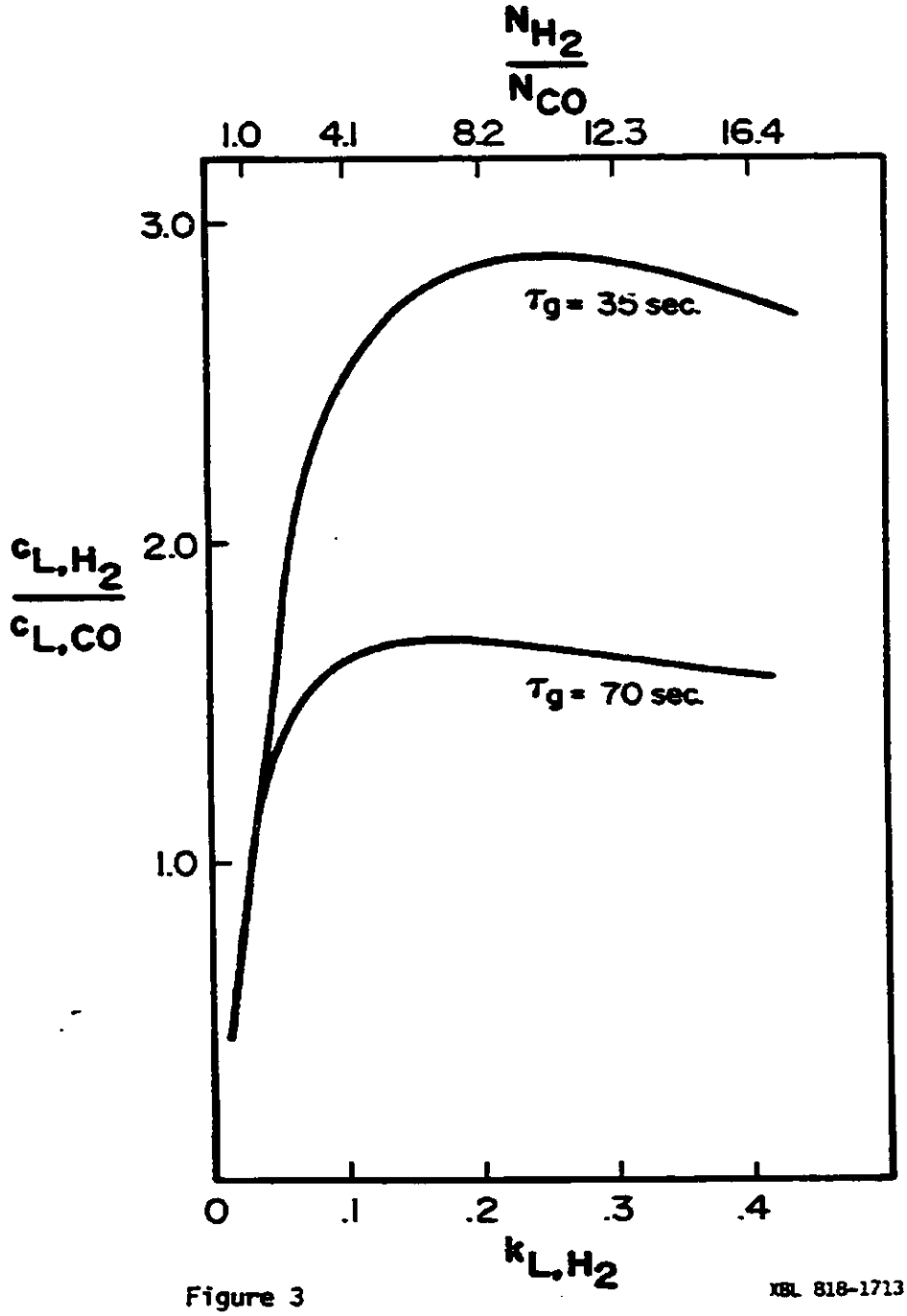

Figure 3

XBL 818-1713

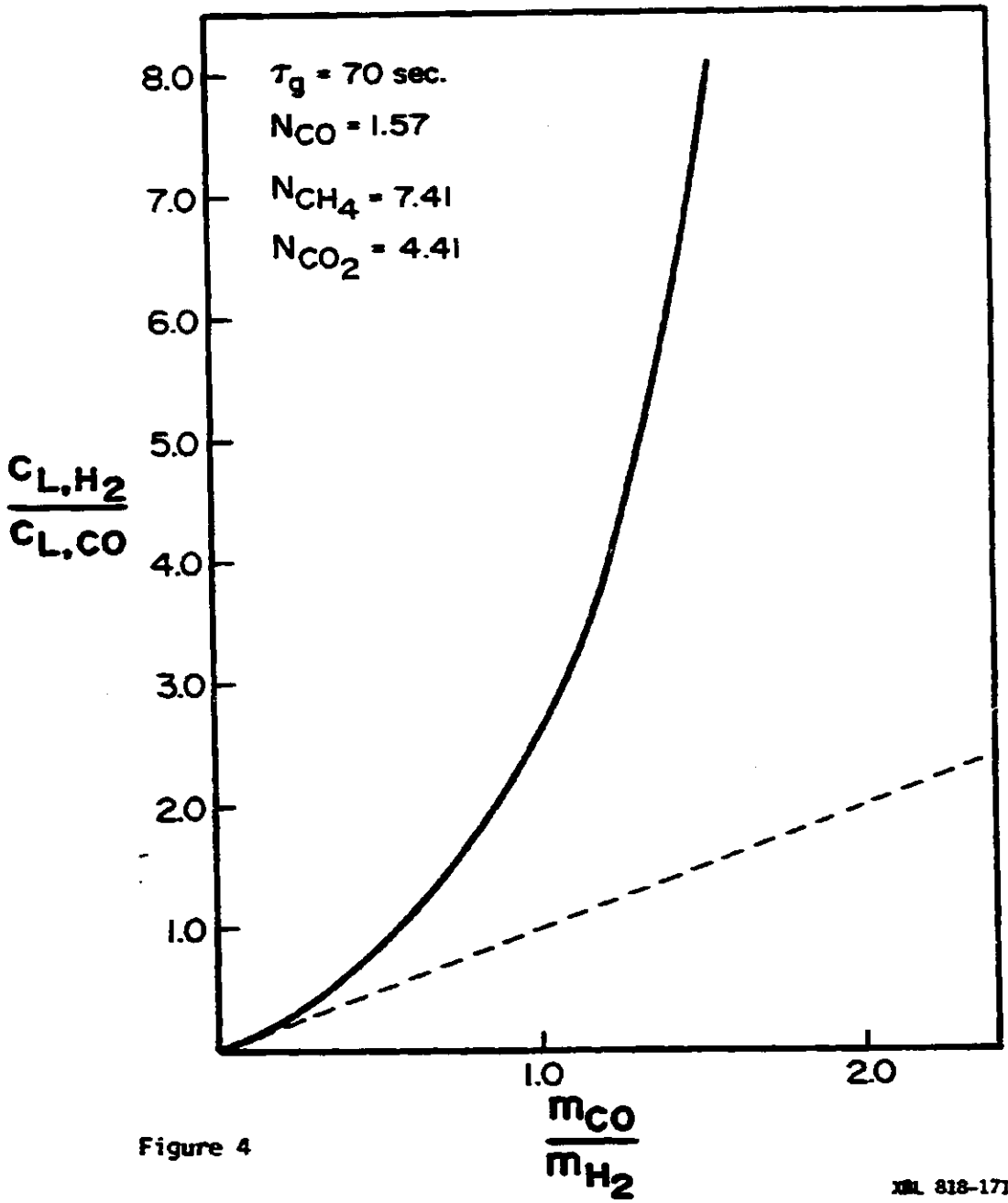

Figure 4

XBL 818-1718

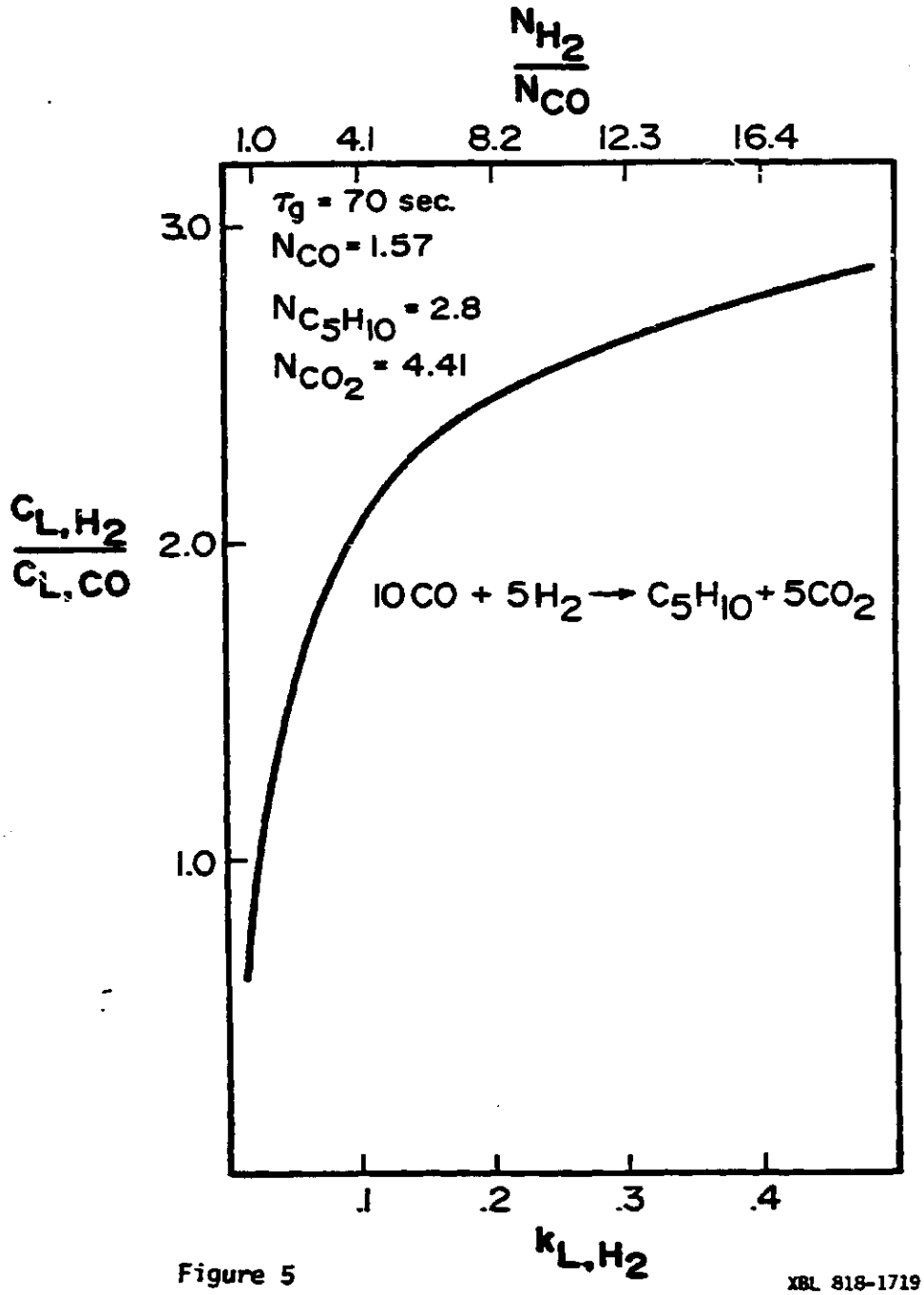

Figure 5

XBL 818-1719